LETTER

doi:10.1038/nature10507

Macrophage skewing by *Phd2* haplodeficiency prevents ischaemia by inducing arteriogenesis

Yukiji Takeda[1,2,3,4], Sandra Costa[1,2,5]*, Estelle Delamarre[1,2]*, Carmen Roncal[1,2,3,4,6]*, Rodrigo Leite de Oliveira[1,2,3,4], Mario Leonardo Squadrito[7,8], Veronica Finisguerra[1,2], Sofie Deschoemaeker[1,2], Françoise Bruyère[3,4], Mathias Wenes[1,2], Alexander Hamm[1,2], Jens Serneels[1,2], Julie Magat[9], Tapan Bhattacharyya[10]†, Andrey Anisimov[11], Benedicte F. Jordan[9], Kari Alitalo[11], Patrick Maxwell[10], Bernard Gallez[9], Zhen W. Zhuang[12], Yoshihiko Saito[13], Michael Simons[12], Michele De Palma[7]† & Massimiliano Mazzone[1,2]

PHD2 serves as an oxygen sensor that rescues blood supply by regulating vessel formation and shape in case of oxygen shortage[1–5]. However, it is unknown whether PHD2 can influence arteriogenesis. Here we studied the role of PHD2 in collateral artery growth by using hindlimb ischaemia as a model, a process that compensates for the lack of blood flow in case of major arterial occlusion[6–8]. We show that *Phd2* (also known as *Egln1*) haplodeficient (*Phd2*$^{+/-}$) mice displayed preformed collateral arteries that preserved limb perfusion and prevented tissue necrosis in ischaemia. Improved arteriogenesis in *Phd2*$^{+/-}$ mice was due to an expansion of tissue-resident, M2-like macrophages[9,10] and their increased release of arteriogenic factors, leading to enhanced smooth muscle cell (SMC) recruitment and growth. Both chronic and acute deletion of one *Phd2* allele in macrophages was sufficient to skew their polarization towards a pro-arteriogenic phenotype. Mechanistically, collateral vessel preconditioning relied on the activation of canonical NF-κB pathway in *Phd2*$^{+/-}$ macrophages. These results unravel how PHD2 regulates arteriogenesis and artery homeostasis by controlling a specific differentiation state in macrophages and suggest new treatment options for ischaemic disorders.

To understand whether partial loss of PHD2 enhances perfusion of ischaemic tissues, we subjected mice to femoral artery ligation, a procedure that reduces perfusion of the lower limb, causing ischaemia in the calf (that is, the crural muscle). After ligation, *Phd2*$^{+/-}$ mice showed a milder drop in perfusion and oxygen tension with reduced hypoxia in the crural muscle compared to wild-type (WT) mice (Fig. 1a–g). Ischaemia promotes oxidative stress early and angiogenesis as a later response[6,11]. Oxidative stress (12 h post-ligation) and capillarization (14 days post-ligation) were both increased in the crural muscle of WT, but not *Phd2*$^{+/-}$ mice (Supplementary Fig. 2a–g). As a consequence of preserved blood flow, *Phd2*$^{+/-}$ crural muscles showed reduced ischaemic necrosis and increased viability (Fig. 1h–j and Supplementary Fig. 2h–j). WT mice showed signs of muscle regeneration that were absent in *Phd2*$^{+/-}$ crural muscles (Supplementary Fig. 2k–m). The protection against ischaemic damage improved physical endurance of *Phd2*$^{+/-}$ mice in ischaemia (Fig. 1k), although both genotypes had similar running capacity at baseline (Supplementary Fig. 2n).

Because *Phd2*$^{+/-}$ mice were protected against ischaemia already 12 h post-ligation, we proposed that they could tolerate ischaemic insults better due to increased collaterals at baseline[12]. Macroscopic inspection of the upper limb, that is, the thigh, and histological analysis of the adductor (in the inner thigh, where collaterals grow) after gelatin-bismuth angiographies showed about twice higher numbers and area of bismuth-positive collaterals in non-ligated *Phd2*$^{+/-}$ versus WT mice (Fig. 1l–q and Supplementary Fig. 3a,b). Also micro-computed tomography scans and X-ray radiographies showed higher numbers of large vessels (>200 μm in diameter) in *Phd2*$^{+/-}$ than WT thighs at baseline (Fig. 1r–t and Supplementary Fig. 3c, d), whereas numbers of smaller vessels (<200 μm in diameter) and capillaries were comparable in both genotypes (Supplementary Fig. 3e–g). Both the total area and numbers of bismuth-positive collaterals were still higher in *Phd2*$^{+/-}$ versus WT adductors 12 and 72 h post-ligation, a time-window when collateral remodelling just begins in WT mice (Fig. 1p, q and Supplementary Fig. 3a, b).

We also assessed whether *Phd2*$^{+/-}$ mice were protected against myocardial ischaemia. Twenty-four hours after coronary artery ligation, desmin-negative area (a readout of cardiomyocyte death) was smaller in *Phd2*$^{+/-}$ hearts (Supplementary Fig. 4a–c). Compared to WT, *Phd2*$^{+/-}$ hearts showed higher perfusion in both infarcted and remote myocardium (Supplementary Fig. 4d–g). At baseline, density of large vessels, but not small vessels and capillaries, was higher in *Phd2*$^{+/-}$ versus WT hearts (Supplementary Fig. 4h–l).

To increase blood flow in case of major arterial occlusion, collateral vessels undergo extensive remodelling (arteriogenesis) with thickening of the tunica media, consisting of α-smooth muscle actin (αSMA)-positive SMCs, and enlargement of vessel diameter[8]. Numbers and total area of αSMA$^+$ collateral vessels were higher in *Phd2*$^{+/-}$ adductors both at baseline and after ischaemia, whereas the mean area and thickness of the tunica media were higher only at baseline (Fig. 1u–b′). These data show that collateral vessels of *Phd2*$^{+/-}$ mice at baseline were similar to those of WT mice after femoral artery ligation. This 'collateral vessel preconditioning' was protective against ischaemia.

Inflammatory cells and macrophages in particular are responsible for collateral vessel remodelling[7,8]. Nevertheless, CD45$^+$ leukocyte and F4/80$^+$ macrophage infiltration of the adductors was similar at baseline and equally increased after ligation in both genotypes (Fig. 2a, b). We therefore analysed the phenotype of infiltrating macrophages and measured the density of M2-like, wound-healing/pro-angiogenic macrophages by their expression of the MRC1 mannose receptor[9,10]. At baseline, F4/80$^+$MRC1$^+$ macrophages were 75% higher in *Phd2*$^{+/-}$ versus WT adductors (Fig. 2c–e). Seventy-two hours after ligation, their numbers were increased by 95% in WT and only 50% in *Phd2*$^{+/-}$ mice

[1]Laboratory of Molecular Oncology and Angiogenesis, Vesalius Research Center, VIB, Leuven B-3000, Belgium. [2]Laboratory of Molecular Oncology and Angiogenesis, Vesalius Research Center, K. U. Leuven, Leuven B-3000, Belgium. [3]Laboratory of Angiogenesis and Neurovascular link, Vesalius Research Center, VIB, Leuven B-3000, Belgium. [4]Laboratory of Angiogenesis and Neurovascular link, Vesalius Research Center, K. U. Leuven, Leuven B-3000, Belgium. [5]Life and Health Sciences Research Institute, Minho University, 4710-057 Braga, Portugal. [6]Atherosclerosis Research Laboratory, CIMA-University of Navarra, 31008 Pamplona, Spain. [7]Angiogenesis and Tumor Targeting Unit and HSR-TIGET, San Raffaele Institute, 20132 Milan, Italy. [8]Vita-Salute University, 20132 Milan, Italy. [9]Biomedical Magnetic Resonance Unit, Universite Catholique de Louvain, Brussels B-1200, Belgium. [10]Rayne Institute, University College London, London WC1E 6JF, UK. [11]Molecular/Cancer Biology Laboratory, Research Programs Unit and Institute for Molecular Medicine, Biomedicum Helsinki, 00014 Helsinki, Finland. [12]Cardiovascular Medicine, Yale University School of Medicine, New Haven, Connecticut 06510, USA. [13]The First Department of Internal Medicine, Nara Medical University, 634-8522 Nara, Japan. †Present addresses: Faculty of Infectious & Tropical Diseases, London School of Hygiene & Tropical Medicine, London WC1E 7HT, UK (T.P.); The Swiss Institute for Experimental Cancer Research (ISREC), Swiss Federal Institute of Technology Lausanne (EPFL), Lausanne, CH-1015, Switzerland (M.D.P.).
*These authors contributed equally to this work.

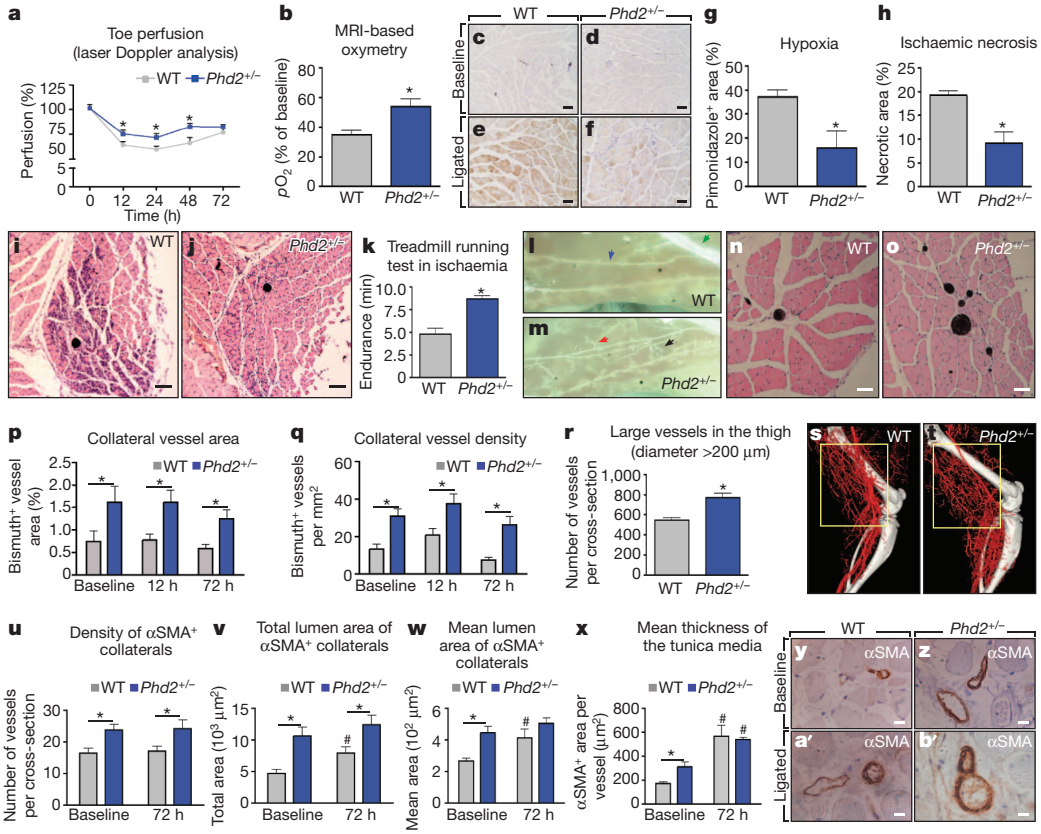

Figure 1 | *Phd2*$^{+/-}$ mice are pre-adapted to ischaemia. **a**, Laser Doppler analysis 12, 24, 48 and 72 h post-ligation. **b**, Magnetic resonance imaging (MRI) oxymetry in crural muscles 12 h post-ligation. **c**–**g**, Hypoxic area quantification (**g**) on pimonidazole-stained sections of crural muscles 12 h post-ligation (**e**, **f**); hypoxia was undetectable at baseline (**c**, **d**). Scale bars, 200 µm. **g**, Pimonidazole^{+} area 12 h post-ligation. **h**–**j**, Necrotic area quantification (**h**) on haematoxylin- and eosin-stained sections of crural muscles 72 h post-ligation (**i**, **j**). Scale bars, 100 µm. **k**, Treadmill running test 12 h post-ligation. **l**, **m**, Macroscopic view of adductors after gelatin-bismuth-based angiographies at baseline. Collateral vessels: primary (blue arrow), secondary (red arrow), and tertiary (black arrow). Femoral artery (green arrow). **n**, **o**, Haematoxylin and eosin staining of adductors at baseline after angiographies; bismuth^{+} collaterals appear black. Scale bars, 50 µm. **p**, **q**, Collateral vessel area (**p**) and density (**q**) represented in **n**, **o**. **r**, Quantification of large vessels (>200 µm in diameter) in the thigh at baseline after micro-computed tomography angiograms. **s**, **t**, Representative micro-computed tomography micrographs of the thigh (yellow frame). **u**–**x**, Morphological analysis on αSMA-stained sections of adductors at baseline and 72 h post-ligation, as represented in **y**–**b′**. Scale bars, 10 µm. All graphs show mean ± s.e.m. All experiments, $n \geq 5$. *, $P < 0.05$ towards WT. #, $P < 0.05$ towards baseline.

(Fig. 2c, f, g). Gene-profiling of *Phd2*$^{+/-}$ peritoneal macrophages (pMØ) showed higher expression of M2-type genes[9,10,13], including *Tek* (also known as *Tie2*), *Arg1*, *Cxcr4*, *Ccr2*, *Hgf*, *Pdgfb*, *Fizz*, *Nrp1*, *Mmp2*, *Cxcl12* (also known as *Sdf1*) and *Tgfb*, than WT pMØ (Fig. 2h). Conversely, several proinflammatory or anti-angiogenic (that is, M1-type) molecules were downregulated in *Phd2*$^{+/-}$ macrophages; these included *Il1b*, *Il6*, *Nos2* and *Il12* (Fig. 2h). Similarly, *Phd2*$^{+/-}$ macrophages sorted from the adductor expressed higher levels of *Pdgfb*, *Sdf1*, *Tie2*, *Mmp2* and *Nrp1* at baseline (Fig. 2i). Seventy-two hours post-ligation, the expression level of these markers was similar in *Phd2*$^{+/-}$ and WT tissue macrophages (Fig. 2i). Expression of these genes was comparable in WT and *Phd2*$^{+/-}$ endothelial cells isolated from adductors at baseline or in ischaemia (Supplementary Table 1). Noteworthy, the basal level of *Phd2* in *Phd2*$^{+/-}$ macrophages was half of that in WT macrophages and did not change in ischaemia (Fig. 2i). Conversely, *Phd2* expression in WT macrophages was reduced by ~50% in ischaemia and thus reached the same level as in *Phd2*$^{+/-}$ macrophages (Fig. 2i). Thus, *Phd2*$^{+/-}$ macrophages showed a unique and cell-specific gene signature, which was reminiscent, at least in part, of M2-polarized macrophages and of WT macrophages in ischaemia.

We therefore assessed whether WT and *Phd2*$^{+/-}$ macrophages affect the behaviour of endothelial cells and SMCs, the two main cellular components of arteries. Soluble factors released by *Phd2*$^{+/-}$ macrophages strongly increased migration and proliferation of SMCs, but not endothelial cells, probably because the latter were already highly responsive to WT macrophages (Fig. 2j–n and Supplementary Fig. 5a–e). Consistently, SMCs exposed to conditioned medium from *Phd2*$^{+/-}$ macrophages showed reduced levels of calponin-1, Sm22, smoothelin, NMHC-B and αSMA (Fig. 2o–s), indicating enhanced proliferation[14,15]. *In vitro* knockdown of both *Sdf1* and *Pdgfb*, known to stimulate SMC recruitment and proliferation[16,17], abolished the enhanced response of SMCs to *Phd2*$^{+/-}$ macrophages, although inhibition of either factor was also very effective (Supplementary Fig. 5f, g and Supplementary Note 1). Overall, these data showed that lower levels of PHD2 pre-adapt macrophages to ischaemia by skewing them towards an M2-like phenotype, which promotes SMC recruitment and growth.

We then investigated whether reduced levels of PHD2 in macrophages promoted collateral vessel preconditioning. Myeloid-cell specific *Phd2* haplodeficiency (*Phd2*$^{LysCre;lox/WT}$) increased numbers and area of collateral branch arteries, thus conferring protection against ischaemic necrosis and enhancing running capacity in ischaemia (Fig. 3a–i and Supplementary Fig. 6a). In myeloid-cell-specific *Phd2*-null mice (*Phd2*$^{LysCre;lox/lox}$), arterialization, ischaemic necrosis and physical endurance were unchanged (Fig. 3a–i and Supplementary Fig. 6a), probably because of the compensatory activity of PHD3, another PHD family member (see below). We also transplanted WT or *Phd2*$^{+/-}$ (hereafter HE for 'heterozygous') bone marrow (BM) cells into irradiated WT (referred to as WT→WT and HE→WT mice, respectively) or *Phd2*$^{+/-}$ (WT→HE and HE→HE mice, respectively) recipients (Supplementary Note 2). Compared to WT→WT, collateral vessel density and area were higher in HE→WT and HE→HE but

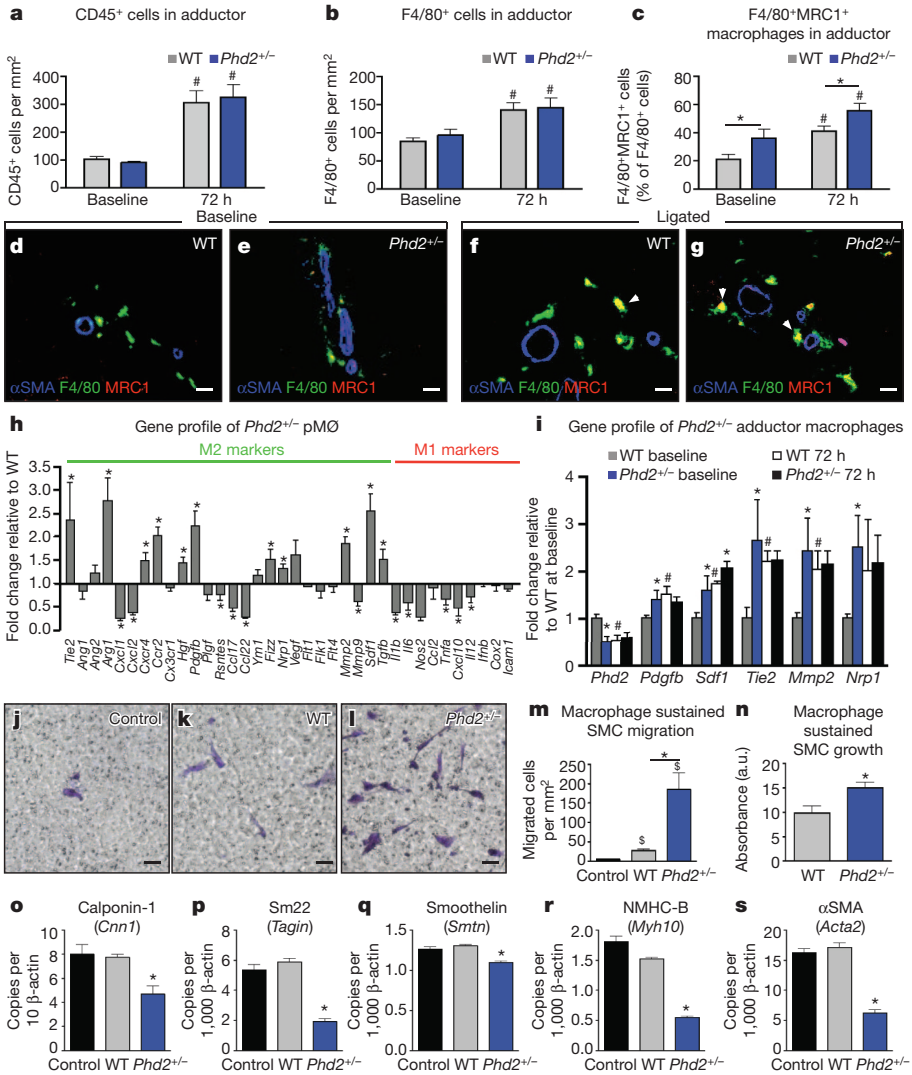

Figure 2 | *Phd2*$^{+/-}$ macrophages display an M2-like phenotype. **a**, **b**, Quantification of CD45^{+} leukocyte and F4/80^{+} macrophage infiltration of adductors at baseline and 72 h post-ligation. **c**, Quantification of MRC1^{+} macrophages in adductors at baseline and 72 h post-ligation, represented in **d**–**g**. **d**–**g**, Micrographs of immunostainings for F4/80 (green), MRC1 (red) and αSMA (blue). Arrowheads (**f**, **g**) point to F4/80^{+}MRC1^{+} cells. Scale bars, 20 μm. **h**, Gene profile by quantitative PCR of peritoneal macrophages (pMØ). **i**, Gene profile of F4/80^{+} macrophages sorted from adductors at baseline and 72 h post-ligation. **j**–**m**, Quantification (**m**) of crystal-violet-stained SMCs, migrated towards control medium (**j**), WT (**k**) or *Phd2*$^{+/-}$ (**l**) macrophages. Scale bars, 50 μm. **n**, SMC growth in response to soluble factors released by WT or *Phd2*$^{+/-}$ macrophages. **o**–**s**, Gene profile by quantitative PCR of SMCs exposed to control, WT macrophage-conditioned medium, or *Phd2*$^{+/-}$ macrophage-conditioned medium. All bars show mean ± s.e.m. All experiments, $n \geq 5$. *, $P < 0.05$ towards WT. #, $P < 0.05$ towards baseline. $, $P < 0.05$ towards control medium.

similar in WT→HE mice, supporting the key role of BM-derived cells in enhancing collateralization and sustaining pre-existing arteries in *Phd2*$^{+/-}$ mice (Fig. 3j, k). In accordance, HE→HE and HE→WT, but not WT→HE mice, were protected against ischaemic necrosis (Fig. 3l). The running capacity of HE→WT mice in ischaemia was twice as high as in WT→WT mice (Fig. 3m and Supplementary Fig. 6b). Deletion of one *Phd2* allele in haematopoietic cells, endothelial cells or SMCs confirmed that enhanced collateral vessel growth and maintenance were specifically conferred by *Phd2* haplodeficiency in BM cells, but not endothelial cells or SMCs (Supplementary Tables 2 and 3). We also assessed the effect of acute deletion of *Phd2* in macrophages by transplanting BM cells from tamoxifen-inducible *Phd2*-haplodeficient mice (*Phd2*$^{Rosa26CreERT;lox/WT}$) into WT recipient mice (HE^{Rosa26CreERT}→WT). Tamoxifen-induced deletion of one *Phd2* allele in BM cells increased collateral branches and protected against ischaemic necrosis when compared to vehicle (Fig. 3n–p and Supplementary Note 3). Thus, both chronic and acute deletion of one *Phd2* allele in myeloid cells was sufficient to induce pro-arteriogenic macrophages, leading to enhanced collaterogenesis and prevention of ischaemia.

PHD oxygen sensors negatively regulate HIF accumulation and NF-κB activity[1,11,18–22]. Compared to WT, HIF-1α and HIF-2α protein levels were respectively four and two times higher in *Phd2*-null macrophages, but unchanged in *Phd2*-haplodeficient macrophages (Fig. 4a). Conversely, NF-κB activity was increased by 65% in *Phd2*-haplodeficient macrophages but unaffected in *Phd2*-null macrophages (Fig. 4b). We proposed that PHD3 might compensate for the complete loss of *Phd2* because *Phd3* transcripts were 12.2-fold higher in *Phd2*-null macrophages (Supplementary Fig. 7). Indeed, *Phd3* silencing resulted in a modest induction of NF-κB activity in WT and *Phd2*-haplodeficient macrophages in contrast to a 70% increase in *Phd2*-null macrophages compared to their scramble controls (Fig. 4b and Supplementary Note 4). PHD2 hydroxylase function was necessary for NF-κB regulation because ectopic expression of a wild-type PHD2 (PHD2^{WT}) greatly blunted the activity of NF-κB luciferase induced by *Phd2* haplodeficiency, whereas a hydroxylase-deficient PHD2 (PHD2^{H313A}) had no effect (Fig. 4c). NF-κB activation by TNF-α was still significantly stronger in *Phd2*$^{+/-}$ macrophages (Fig. 4d). In contrast, basal and TNF-α-induced NF-κB activity were similar in WT and *Phd2*$^{+/-}$ endothelial cells (Supplementary Fig. 8a). When measuring the nuclear accumulation of NF-κB subunits, we found that members of the canonical pathway, that is, p65 (RelA) and p50 (NF-κB1), were more abundant in *Phd2*$^{+/-}$ than WT macrophages (Fig. 4e). Silencing of p65 or p50 blocked NF-κB hyperactivation in *Phd2*$^{+/-}$ macrophages and the combined knockdown of both subunits restored NF-κB function back to WT levels (Fig. 4f and Supplementary Note 5), thus highlighting the prominent role of NF-κB p65/p50 heterodimers in *Phd2*$^{+/-}$ macrophages. To evaluate the involvement of canonical NF-κB signalling in macrophage skewing by *Phd2* haplodeficiency, we generated a myeloid-cell specific double transgenic strain, haplodeficient for *Phd2* and null for *Ikbkb*, the gene encoding IKKβ, a positive regulator of canonical NF-κB pathway. Genetic disruption (or pharmacological inhibition) of canonical NF-κB pathway prevented the upregulation

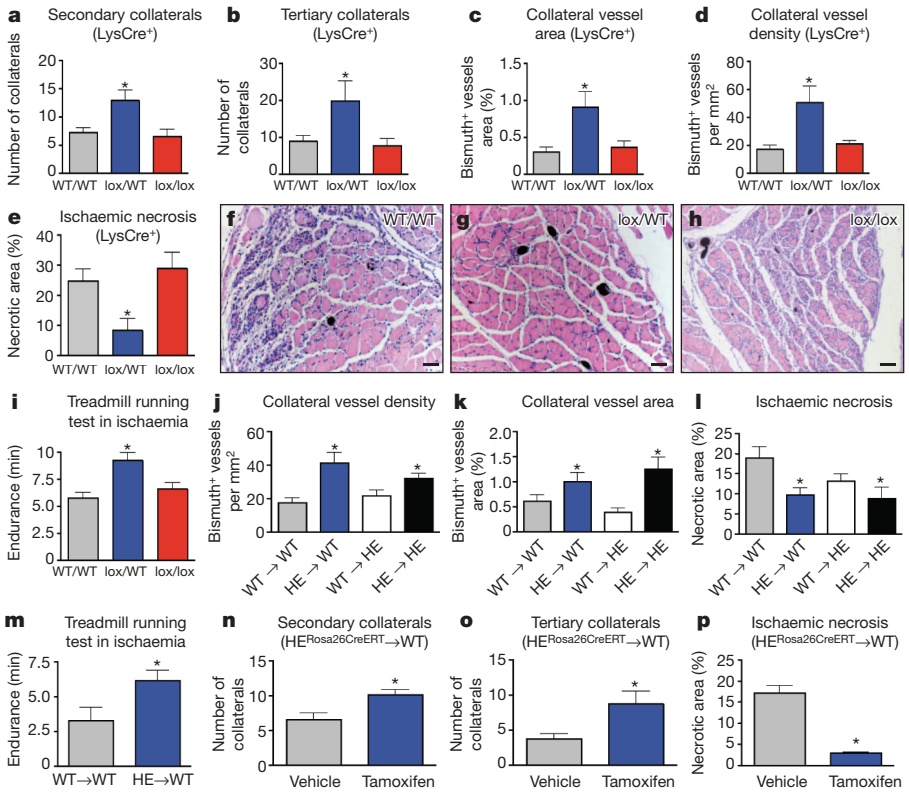

Figure 3 | *Phd2*$^{+/-}$ macrophages protect against ischaemia by inducing arteriogenesis. **a**, **b**, Quantification of secondary (**a**) and tertiary (**b**) collateral branches in WT (*Phd2*$^{LysCre;WT/WT}$; WT/WT), myeloid-cell specific *Phd2*-haplodeficient (*Phd2*$^{LysCre;lox/WT}$; lox/WT) or null mice (*Phd2*$^{LysCre;lox/lox}$; lox/lox). **c**, **d**, Bismuth$^+$ collateral vessel area (**c**) and density (**d**) of adductors at baseline. **e**–**h**, Necrotic area quantification (**e**) on haematoxylin- and eosin-stained sections of crural muscles 72 h post-ligation (**f**–**h**). Scale bars, 100 μm. **i**, Treadmill running test 12 h post-ligation. **j**, **k**, Bismuth$^+$ collateral vessel density (**j**) and area (**k**) of non-occluded limbs 5 weeks after bone marrow (BM) transplantation. *Phd2*$^{+/-}$ BM in WT and *Phd2*$^{+/-}$ recipient mice (HE→WT and HE→HE, respectively); WT BM in WT and *Phd2*$^{+/-}$ recipient mice (WT→WT and WT→HE). **l**, Ischaemic necrosis 72 h post-ligation. **m**, Treadmill running test 12 h post-ligation in WT→WT and HE→WT mice. **n**–**p**, Quantification of secondary (**n**) and tertiary (**o**) collateral vessels at baseline and of ischaemic necrosis 72 h post-ligation (**p**), following tamoxifen-induced deletion of one *Phd2* allele in BM cells of HE^{Rosa26CreERT}→WT mice. All bars show mean ± s.e.m. All experiments, $n \geq 4$. *, $P < 0.05$ towards WT/WT and lox/lox in **a**–**i**, towards WT→WT in **j**–**m**, or towards vehicle in **n**–**p**.

of *Pdgfb* and *Sdf1* in cultured *Phd2*-haplodeficient macrophages (Fig. 4g and Supplementary Fig. 8b). *In vivo*, gene inactivation of *Ikbkb* in myeloid cells abolished collateral vessel preconditioning conferred by *Phd2* haplodeficiency and greatly prevented ischaemia-induced arteriogenesis in WT mice (Fig. 4h). Thus, skewing of *Phd2*-haplodeficient macrophages towards a pro-arteriogenic phenotype relied on activation of canonical NF-κB pathway.

Specific macrophage differentiation states have been implicated in the promotion of angiogenesis during cancer and atherosclerosis progression[9,10,13,23]. However, little is known of the significance of macrophage heterogeneity in arteriogenesis and its implications on ischaemic diseases. This study identifies a role of macrophage PHD2 in oxygen delivery by regulating arteriogenesis. We show that the phenotype of macrophages induced by reduced PHD2 levels not only favours the formation of new collateral branches, but is also important for collateral vessel homeostasis (Supplementary Note 6). In our model, ischaemia favours the accumulation of M2-like, pro-arteriogenic macrophages that fuel collateral vessel maturation in a NF-κB-dependent manner (Supplementary Fig. 1). *Phd2* haplodeficiency unleashes constitutive

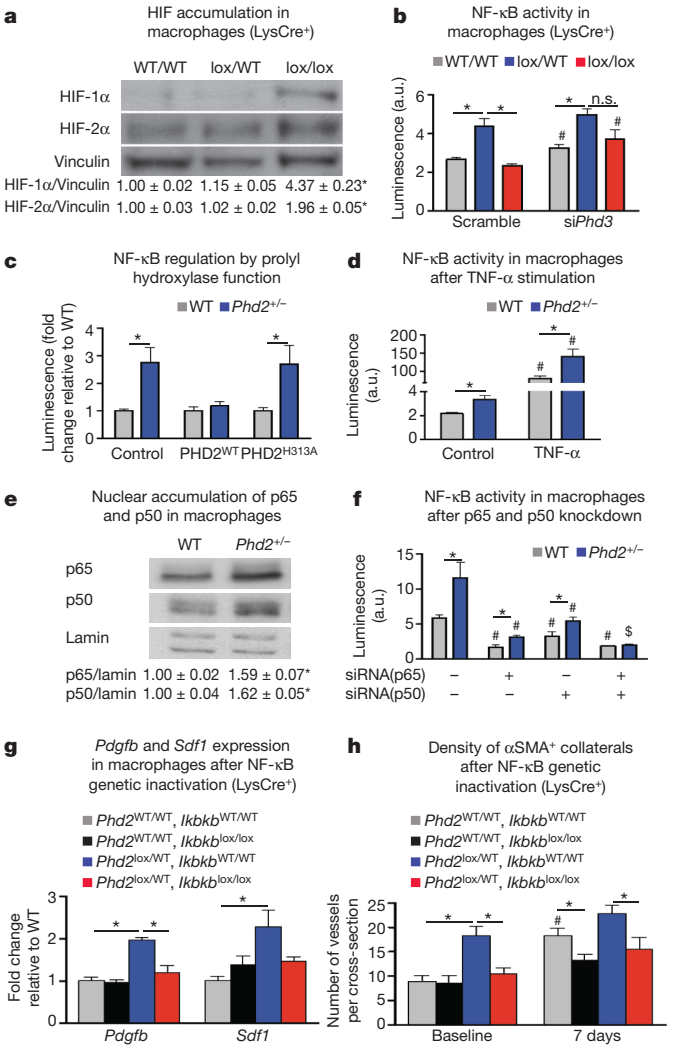

Figure 4 | *Phd2*$^{+/-}$ macrophages trigger arteriogenesis via canonical NF-κB pathway. **a**, Western blot for HIF-1α and HIF-2α in WT (WT/WT), *Phd2*-haplodeficient (lox/WT) and *Phd2*-null (lox/lox) macrophages. Vinculin was used as loading control. Numbers represent densitometric fold change towards WT/WT. **b**, NF-κB activity in macrophages after *Phd3* silencing (si*Phd3*; n.s., not significant). **c**, NF-κB activity in *Phd2*$^{+/-}$ macrophages upon ectopic expression of wild-type PHD2 (PHD2^{WT}) or hydroxylase-deficient PHD2 (PHD2^{H313A}). **d**, NF-κB activity in macrophages at baseline and upon TNF-α stimulation. **e**, Western blot for nuclear p65 and p50 in WT and *Phd2*$^{+/-}$ macrophages. Numbers represent densitometric fold change towards WT. **f**, NF-κB activity in macrophages after silencing of p65, p50, or combination of both. **g**, *Pdgfb* and *Sdf1* expression (quantitative PCR) after genetic inactivation of *Ikbkβ* in *Phd2*-haplodeficient pMØ (*Phd2*$^{lox/WT}$,*Ikbkb*$^{lox/lox}$). **h**, Quantification of αSMA$^+$ collaterals in myeloid-cell-specific *Phd2*-haplodeficient and *Ikbkb*-null mice at baseline and 7 days post-ligation. All bars and values show mean ± s.e.m. All experiments, $n \geq 4$. *, $P < 0.05$ towards wt/wt in **a**, **b**, **g**, **h**, or towards WT in **c**–**f**. #, $P < 0.05$ towards scramble in **b**, **f**, or towards baseline in **d**, **h**. $, $P < 0.05$ towards scramble and either short interfering RNA alone.

NF-κB signals that pre-adapt tissue-resident macrophages to ischaemia, accounting for the enhanced arteriogenesis at baseline and thus protection against ischaemic tissue demise. In particular, we show that NF-κB activation in *Phd2*$^{+/-}$ macrophages increases the production of SDF1 and PDGFB, which are concurrently required to prime SMC migration and growth *in vitro*. The relevance of SDF1 and PDGFB *in vivo* remains to be established, and other soluble factors may also contribute.

Repression of canonical NF-κB pathway in macrophages promotes upregulation of M1-type and downregulation of M2-type genes[24–26]. PHDs negatively regulate NF-κB through either hydroxylase-dependent or -independent inactivation of IKKβ in different cell contexts[19–22]. We show here that *Phd2* haplodeficiency results in hyperactivation of canonical NF-κB pathway in macrophages and promotion of the M2-phenotype via accumulation of both p65 and p50 subunits, and that this regulation requires PHD hydroxylase function.

In summary, our study provides an insight on how the PHD2 oxygen sensor regulates arteriogenesis by modulating macrophage phenotype. The mechanism upstream to arteriogenic PHD2 downregulation in M2-like macrophages remains to be established. Nonetheless, our findings support the rationale for therapeutic inhibition of PHD2. Previous studies showed that unspecific inhibitors of PHD2 or silencing of PHD2 promote therapeutic revascularization against ischaemia[2–5]. However, angiogenesis is a late response and organ function might be compromised before new blood vessel formation is achieved. In contrast, arteriogenesis takes place on pre-existing vascular shunts and our data suggest that either PHD2 inhibitors or cell-therapy-based strategies using PHD2 hypomorphic macrophages might be exploited as preventive medicine to promote collateral vascularization in patients at risk of limb or heart ischaemia, such as diabetic or hypercholesterolemic patients.

METHODS SUMMARY

129/S6 or Balb/c WT and *Phd2*$^{+/-}$ mice (8–12 weeks old) were obtained from our mouse facility. *Phd2*$^{+/-}$ and *Phd2* conditional knockout mice were obtained as previously described[1]. To induce hindlimb ischaemia, unilateral or bilateral ligations of the femoral artery and vein and the cutaneous vessels branching from the caudal femoral artery side branch were performed without damaging the nervus femoralis[27]. Oxygen tension (pO_2) in the lower limb was measured 12 h after femoral artery ligation by ^{19}F magnetic resonance imaging oxymetry. Adductors and crural muscles were dissected, fixed in 2% paraformaldehyde, dehydrated, embedded in paraffin and sectioned at 7-μm thickness for histology, immunostaining and morphometry analysis. Macrophages were either collected from the peritoneal cavity of the mice (pMØ) or derived from BM precursors as described before[28]. Balb/c WT and *Phd2*$^{+/-}$ recipient mice were irradiated with 7.5 Gy. Subsequently, 5×10^6 BM cells from green fluorescent protein$^+$ (GFP$^+$) WT or GFP$^+$ *Phd2*$^{+/-}$ mice were injected intravenously via the tail vein. Femoral artery ligation, treadmill running test and bismuth angiography were performed 5 weeks after BM reconstitution. Full Methods and any associated references are available in the Supplementary Information.

Full Methods and any associated references are available in the online version of the paper at www.nature.com/nature.

Received 22 September 2010; accepted 23 August 2011.
Published online 9 October 2011.

1. Mazzone, M. *et al.* Heterozygous deficiency of PHD2 restores tumor oxygenation and inhibits metastasis via endothelial normalization. *Cell* **136,** 839–851 (2009).
2. Milkiewicz, M., Pugh, C. W. & Egginton, S. Inhibition of endogenous HIF inactivation induces angiogenesis in ischaemic skeletal muscles of mice. *J. Physiol. (Lond.)* **560,** 21–26 (2004).
3. Nangaku, M. *et al.* A novel class of prolyl hydroxylase inhibitors induces angiogenesis and exerts organ protection against ischemia. *Arterioscler. Thromb. Vasc. Biol.* **27,** 2548–2554 (2007).
4. Huang, M. *et al.* Short hairpin RNA interference therapy for ischemic heart disease. *Circulation* **118,** S226–S233 (2008).
5. Loinard, C. *et al.* Inhibition of prolyl hydroxylase domain proteins promotes therapeutic revascularization. *Circulation* **120,** 50–59 (2009).
6. Carmeliet, P. Mechanisms of angiogenesis and arteriogenesis. *Nature Med.* **6,** 389–395 (2000).
7. Simons, M. & Ware, J. A. Therapeutic angiogenesis in cardiovascular disease. *Nature Rev. Drug Discov.* **2,** 863–872 (2003).
8. Schaper, W. Collateral circulation: past and present. *Basic Res. Cardiol.* **104,** 5–21 (2009).
9. Mantovani, A. & Sica, A. Macrophages, innate immunity and cancer: balance, tolerance, and diversity. *Curr. Opin. Immunol.* **22,** 231–237 (2010).
10. Nucera, S., Biziato, D. & De Palma, M. The interplay between macrophages and angiogenesis in development, tissue injury and regeneration. *Int. J. Dev. Biol.* **55,** 495–503 (2011).
11. Aragonés, J. *et al.* Deficiency or inhibition of oxygen sensor Phd1 induces hypoxia tolerance by reprogramming basal metabolism. *Nature Genet.* **40,** 170–180 (2008).
12. Helisch, A. *et al.* Impact of mouse strain differences in innate hindlimb collateral vasculature. *Arterioscler. Thromb. Vasc. Biol.* **26,** 520–526 (2006).
13. Squadrito, M. L. & De Palma, M. Macrophage regulation of tumor angiogenesis: Implications for cancer therapy. *Mol. Aspects Med.* **32,** 123–145 (2011).
14. Kumar, M. S. & Owens, G. K. Combinatorial control of smooth muscle-specific gene expression. *Arterioscler. Thromb. Vasc. Biol.* **23,** 737–747 (2003).
15. Wolf, C. *et al.* Vascular remodeling and altered protein expression during growth of coronary collateral arteries. *J. Mol. Cell. Cardiol.* **30,** 2291–2305 (1998).
16. Karshovska, E., Zagorac, D., Zernecke, A., Weber, C. & Schober, A. A small molecule CXCR4 antagonist inhibits neointima formation and smooth muscle progenitor cell mobilization after arterial injury. *J. Thromb. Haemost.* **6,** 1812–1815 (2008).
17. Hellstrom, M., Kalen, M., Lindahl, P., Abramsson, A. & Betsholtz, C. Role of PDGF-B and PDGFR-β in recruitment of vascular smooth muscle cells and pericytes during embryonic blood vessel formation in the mouse. *Development* **126,** 3047–3055 (1999).
18. Jaakkola, P. *et al.* Targeting of HIF-α to the von Hippel-Lindau ubiquitylation complex by O_2-regulated prolyl hydroxylation. *Science* **292,** 468–472 (2001).
19. Chan, D. A. *et al.* Tumor vasculature is regulated by PHD2-mediated angiogenesis and bone marrow-derived cell recruitment. *Cancer Cell* **15,** 527–538 (2009).
20. Xue, J. *et al.* Prolyl hydroxylase-3 is down-regulated in colorectal cancer cells and inhibits IKKβ independent of hydroxylase activity. *Gastroenterology* **138,** 606–615 (2010).
21. Cummins, E. P. *et al.* Prolyl hydroxylase-1 negatively regulates IκB kinase-β, giving insight into hypoxia-induced NFκB activity. *Proc. Natl Acad. Sci. USA* **103,** 18154–18159 (2006).
22. Fu, J. & Taubman, M. B. Prolyl hydroxylase EGLN3 regulates skeletal myoblast differentiation through an NF-κB-dependent pathway. *J. Biol. Chem.* **285,** 8927–8935 (2010).
23. Mantovani, A., Garlanda, C. & Locati, M. Macrophage diversity and polarization in atherosclerosis: a question of balance. *Arterioscler. Thromb. Vasc. Biol.* **29,** 1419–1423 (2009).
24. Fong, C. H. *et al.* An antiinflammatory role for IKKβ through the inhibition of "classical" macrophage activation. *J. Exp. Med.* **205,** 1269–1276 (2008).
25. Hagemann, T. *et al.* "Re-educating" tumor-associated macrophages by targeting NF-κB. *J. Exp. Med.* **205,** 1261–1268 (2008).
26. Greten, F. R. *et al.* NF-κB is a negative regulator of IL-1β secretion as revealed by genetic and pharmacological inhibition of IKKβ. *Cell* **130,** 918–931 (2007).
27. Luttun, A. *et al.* Revascularization of ischemic tissues by PlGF treatment, and inhibition of tumor angiogenesis, arthritis and atherosclerosis by anti-Flt1. *Nature Med.* **8,** 831–840 (2002).
28. Meerpohl, H. G., Lohmann-Matthes, M. L. & Fischer, H. Studies on the activation of mouse bone marrow-derived macrophages by the macrophage cytotoxicity factor (MCF). *Eur. J. Immunol.* **6,** 213–217 (1976).

Supplementary Information is linked to the online version of the paper at www.nature.com/nature.

Acknowledgements This work was supported by grants from FWO (G.0726.10), Belgium, and from VIB. The authors are thankful to P. Carmeliet for the *Phd2* KO and cKO mice, M. Karin for the *Ikbkb* cKO mice, P. Ratcliffe for the PHD2^{H313A} construct, A. Luttun and P. Fazzari for comments, Y. Jonsson and T. Janssens for technical assistance. VE-Cadherin:CreERT and PDGFRB:Cre transgenic mice were generated at Cancer Research UK and kindly donated by R. Adams. E.D. was funded by ARC, S.C. by FCT, R.L.O. and V.F. by FWO, A.H. by DFG. C.R. was supported by COST action TD0901. M.D.P. was supported by an ERC starting grant.

Author Contributions Y.T., E.D. and S.C. performed experimental design, all experiments, acquisition of data and analysis and interpretation of all data. C.R. performed analysis of histological stainings, angiographies. R.L.O., C.R. and S.C. performed the western blots. R.L.O. and V.F. performed treadmill-running tests, quantitative PCR experiments and drug administrations. M.L.S. performed lentiviral vector preparation and cell transduction. F.B. performed EC isolation and angiography measurements. J.M., B.F.J. and B.G. performed oxymetry experiments. S.D. performed luciferase assays. M.W. and A.H. performed transplantation experiments and electroporations. Y.T. and J.S. performed the ligations of the femoral artery. Z.W.Z. and M.S. performed micro-computer tomography angiograms. A.A. and K.A. contributed vital reagents. T.B. and P.M. contributed in generating the *Phd2* targeting vector. Y.T., E.D., S.C., C.R., Y.S. and M.D.P. participated in scientific discussion and drafting of the manuscript. M.M. performed experimental design, data analysis, conducted scientific direction and wrote the manuscript.

Author Information Reprints and permissions information is available at www.nature.com/reprints. The authors declare no competing financial interests. Readers are welcome to comment on the online version of this article at www.nature.com/nature. Correspondence and requests for materials should be addressed to M.M. (massimiliano.mazzone@vib-kuleuven.be)

METHODS

Animals. 129/S6 or Balb/c, female and male, WT and *Phd2*$^{+/-}$ mice (8–12 weeks old) were obtained from our mouse facility. *Phd2*$^{+/-}$ and *Phd2* conditional knockout mice were obtained as previously described[1]. VE-Cadherin:CreERT and PDGFRB:Cre transgenic mice were generated by R. Adams at the Cancer Research UK[29,30]. *Ikbkb* conditional knockout mice were obtained from M. Karin[31]. Tie2:Cre and Rosa26:CreERT transgenic mice were purchased from the Jackson Laboratory. Housing and all experimental animal procedures were performed in accordance with Belgian law on animal care and were approved by the Institutional Animal Care and Research Advisory Committee of the K. U. Leuven (P036/2009).

Mouse model of hindlimb ischaemia and myocardial infarction. To induce hindlimb ischaemia, unilateral or bilateral ligations of the femoral artery and vein (proximal to the popliteal artery) and the cutaneous vessels branching from the caudal femoral artery side branch were performed without damaging the nervus femoralis. By using this procedure, collateral flow to adductor muscles is preserved via arterioles branching from the femoral artery, therefore 50% up to 60% of perfusion is preserved by this method. Two superficial pre-existing collateral arterioles, connecting the femoral and saphenous artery, were used for analysis. Functional perfusion measurements of the collateral region were performed using a Lisca PIM II camera (Gambro). Gelatin-bismuth-based angiography was performed as described before and analysed by photoangiographs (Nikon D1 digital camera). Collateral side branches were categorized as follows: secondary collateral arterioles directly branched from the primary collateral, and tertiary arterioles orientated perpendicularly to the secondary branches. The number of secondary and tertiary collateral arterioles was counted. After perfusion-fixation, the muscle tissue between the two superficial collateral arterioles (adductor) was post-fixed in 2% paraformaldehyde, paraffin-embedded and morphometrically analysed[27]. An endurance treadmill-running test was performed at baseline and 12 h post-bilateral-ligation. Myocardial infarction was induced by permanent ligation of the left anterior descending coronary artery as previously described[32]. Briefly, the left thorax of anesthetized mice was opened in the fourth intercostal space and all the muscles overlying the intercostal region were dissected. The main left anterior descending coronary artery was ligated proximal to the main bifurcation though a small incision of the pericardium. Discoloration of the ventricle after blood flow restriction was used as readout of a successful surgical procedure. Gelatin-bismuth-based angiography was performed 24 h post-ligation and the entire heart was fixed in 2% paraformaldehyde.

Oxymetry. Oxygen tension (pO_2) in the lower limb was measured using ^{19}F-MRI oxymetry in non-ligated and ligated legs 12 h after femoral artery ligation. The oxygen reporter probe hexafluorobenzene was injected directly into the crural muscle. Magnetic resonance imaging was performed with a 4.7 T (200 MHz, ^{1}H), 40-cm inner diameter bore system (Bruker Biospec). A tunable ^{1}H/^{19}F surface coil was used for radiofrequency transmission and reception[33].

Histology, immunostaining, and morphometry. Adductor, crural muscles and hearts were dissected, fixed in 2% paraformaldehyde, dehydrated, embedded in paraffin, and sectioned at 7-μm thickness. Area of necrotic tissues in the crural muscle was analysed by haematoxylin and eosin staining. Necrotic cells display a more glassy homogeneous appearance in the cytoplasm with increased eosinophilia, whereas the nuclear changes are reflected by karyolysis, pyknosis and karyorrhexis. Necrotic area was defined as the percentage of area which includes these necrotic myocytes, inflammatory cells and interstitial cells, compared to the total soleus area. Infarct size was measured in desmin-stained hearts 24 h after ischaemia as previously described[34]. After deparaffinization and rehydration, sections were blocked and incubated overnight with primary antibodies: rat anti-CD31, dilution 1/500 (BD-pharmingen); mouse anti-aSMA, dilution 1/500 (Dako); rat anti-F4/80, dilution 1/100 (Serotec); dilution 1/50 (BD-pharmingen); rat anti-CD45, dilution 1/100 (BD-pharmingen); goat anti-MRC1, dilution 1/200 (R&D); rabbit anti-desmin dilution 1/150 (Cappel). To analyse capillary density and area, images of anti-CD31-stained sections of the entire soleus were taken at ×40. To measure bismuth-positive vessel density and area, haematoxylin- and eosin-stained paraffin sections were analysed and vessels filled with bismuth-gelatin (black spots) were taken in account. Images of the entire soleus were acquired at ×20 for this analysis. The values in the graph represent the averages of the mean vessel density and area per soleus muscle. The same method was used to quantify vessel capillaries and collateral branches in cardiac tissues. Density and area were measured by using a KS300 (Leica) software analysis. Hypoxic cells were analysed 2 h after injection of 60 mg kg^{-1} pimonidazole into operated mice. Mice were killed and muscles were collected. Paraffin sections were stained with Hypoxiprobe-1-Mab-1 (Hypoxiprobe kit; Chemicon International) following the manufacturer's instructions. Oxidative stress and proliferation rate were assessed on 7-μm thick cryosections by using the goat anti-8-OHdG antibody, dilution 1/200 (Serotec) and the rat anti-BrdU antibody, dilution 1/300 (Serotec). Sections were subsequently incubated with appropriate secondary antibodies, developed with fluorescent dies or 3,3′-disminobenzidine (DAB, Sigma). Whole-muscle viability was assessed on unfixed 2-mm thick tissue slices by staining with 2,3,5-triphenyltetrazolium chloride (TTC). Viable area, stained in red, was traced and analysed. Pictures for morphometric analysis were taken using a Retiga EXi camera (Q Imaging) connected to a Nikon E800 microscope or a Zeiss Axio Imager connected to an Axiocam MRc5 camera (Zeiss) and analysis was performed using KS300 (Leica). Angiograms were obtained by X-ray and micro-computed tomography angiographies of hearts and legs at baseline.

Macrophage preparation. To harvest peritoneal macrophages (pMØ), the peritoneal cavity was washed with 5 ml of RPMI 10% FBS. The pooled cells were then seeded in RPMI 10% FBS in 6-well plates (2×10^6 cells per well), 12-well plates (1×10^6 cells per well), or 24-well plates (5×10^5 cells per well). After 6 h of incubation at 37 °C in a moist atmosphere of 5% CO_2 and 95% air, non-adhering cells on each plate were removed by rinsing with phosphate-buffered saline (PBS). The attached macrophages were grown in different media for 12 h or 48 h depending on the experiments performed, as described below. When high amounts of cells were needed (analysis for HIF accumulation and NF-κB activity), macrophages were derived from bone marrow (BM) precursors as described before[28]. Briefly, BM cells (2×10^6 cells per ml) were grown in a volume of 5 ml in a 10-cm Petri dish (non tissue culture treated, bacterial grade) for 7 to 10 days in DMEM supplemented with 20% FBS and 30% L929 conditioned medium as a source of M-CSF. The cells obtained in those cultures are uniformly macrophages.

Quantitative PCR analysis. In order to investigate gene expression in pMØ, quantitative real-time PCR (qPCR) was performed. After preparing pMØ, the cells were cultured in normoxic condition for 12 h and RNA was extracted. To analyse the expression levels of chemoattractants in the adductor, tissues were collected at baseline or 24 h post-ischaemia and RNA was extracted. Macrophages and endothelial cells were freshly sorted from dissected adductors as described below and RNA was extracted. Quantitative PCR was performed with commercially available or home-made primers and probes for the studied genes. The assay ID (Applied Biosystems) or the sequence of primers and probes (when custom-made) are listed in Supplementary Table 4. RNA levels of *Sdf1* and *Pdgfb* after inhibition of NF-κB pathway were measured by qPCR on pMØ exposed for 12 h to 500 nM 6-amino-4-(4-phenoxyphenylethylamino)quinazoline.

Protein extraction and immunoblot. Protein extraction was performed using 8 M urea buffer (10% glycerol, 1% SDS, 5 mM DTT, 10 mM Tris-HCl, pH 6.8) as previously described[1]. Nuclear proteins were extracted in 1% SDS buffer upon cytoplasmic separation by using a hypotonic lysis buffer (10 mM KCl, 10 mM EDTA, 0.5% NP40, 10 mM HEPES, pH 8, supplemented with phosphatase and protease inhibitors, from Roche). Signal was detected using the ECL system (Invitrogen) according to the manufacturer's instructions. The following antibodies were used: rabbit anti-HIF-1α (Novus), rabbit anti-p105/50, rabbit anti-HIF-2α (Abcam), PM9 rabbit anti-HIF-2α (from P.M.), mouse anti-vinculin (Sigma), rabbit anti-lamin A/C, rabbit anti-p65 (Cell Signaling). Densitometric analysis was performed using ImageJ 1.44 (http://rsbweb.nih.gov/ij/).

Transduction and transfection of BM-derived macrophages and lung endothelial cells. To express an inducible NF-κB-responsive firefly luciferase reporter, commercially available lentiviral vectors (LV) were used (Cignal Lenti NF-κB Reporter; SABiosciences). BM-derived macrophages (2.5×10^5) and 10^5 primary lung endothelial cells, isolated as described before[1], were seeded in a 24-well plate in DMEM 10% FBS or M199 20% FBS for 8 h. Cells were transduced with 10^8 transducing units per ml. Eight hours after transduction, the medium was replaced. After 48 h, cells were stimulated with TNF-α (20 ng ml^{-1}) for 8 h and the same amount of protein extract was read in a luminometer. For PHD3 silencing, siRNA oligonucleotides were designed using the Invitrogen online siRNA design tool (http://rnaidesigner.invitrogen.com). The following siRNA sequences (sense strands) were used. For *Egln3/Phd3* (NM_028133.2): 5′-GCCGGCTGGGCAAAT ACTATGTCA-3′; for the scramble: 5′-CACCGCTTAACCCGTATTGCCTAT-3′. In brief, one day after the transduction of macrophages with LV, cells were transfected using Lipofectamine 2000 (Invitrogen) according to the manufacturer's instructions. Preparation of the oligonucleotide–Lipofectamine 2000 complexes was done as follows: 25 pmol siRNA oligonucleotide (stock 20 μM) was diluted in 50 μl Opti-MEM I reduced serum medium. Lipofectamine 2000 (1.5 μl) was diluted in 50 μl Opti-MEM I reduced serum medium and incubated for 5 min at room temperature. siRNA oligonucleotides were gently mixed with Lipofectamine 2000 and allowed to incubate at room temperature for 20 min to form complexes. Just before transfection, the cell culture medium was removed and cells were rinsed twice with serum-free Opti-MEM I medium. The Lipofectamine 2000-siRNA oligonucleotide complexes were added to each well in 400 μl of serum-free Opti-MEM medium for 5 h. Afterwards, cells were incubated in complete medium for 48 h at 37 °C in a CO_2 incubator and assayed for gene knockdown (qPCR) and luciferase activity. To assess if the increased NF-κB activity observed in *Phd2*$^{+/-}$ macrophages was dependent on the hydroxylase activity of PHD2, 48 h before transduction,

4×10^6 BM-derived macrophages were resuspended in 240 µl of Opti-MEM and were electroporated (250 V, 950 µF, $\infty\,\Omega$) with 7 µg of plasmids expressing a wild-type PHD2 ($PHD2^{wt}$) or a PHD2 containing a mutation at the catalytic site ($PHD2^{H313A}$). Silencing of the canonical pathway subunits p65 (*Rela*) and p50 (*Nfkb1*) was achieved by electroporation with specific siRNAs. Briefly, 48 h before transduction, 2.4×10^6 BM-derived macrophages were resuspended in 320 µl of Opti-MEM and were electroporated (250 V, 950 µF, $\infty\,\Omega$) with 60 pmol of siRNA for either scramble, p65, p50, or combination of p50 and p65. For higher efficiency of silencing, two different siRNA sequences for each respective gene were designed (http://rnaidesigner.invitrogen.com). For p65 (NM_009045.4): 5′-TGTCTGCACC TGTTCCAAATT-3′ and 5′-TGCTGATGGAGTACCCTGATT-3′; for p50 (NM_008689.2): 5′-GAATACTTCATGTGACTAATT-3′ and 5′-CAAAGGTTAT CGTTCAGTTTT-3′; for the scramble: 5′-CACCGCTTAACCCGTATTGCCTAT-3′.

Cell migration and viability assays. Migration and proliferation of smooth muscle cells (SMCs) and endothelial cells were assessed by using 8-µm-pore Transwell permeable plate for migration assays and 0.4-µm-pore Transwell permeable plate for proliferation assays (Corning Life Science). To determine cell migration and proliferation in response to soluble factors secreted by pMØ, pMØ were pre-cultured in the lower chamber for 12 h in RPMI 1% FBS or in M-199 1% FBS (migration assay), or 48 h in DMEM-F12 1% FBS or in M-199 1% FBS (proliferation assay). For migration assays, hCASMCs (human coronary artery SMCs; from Lonza) and HUVECs (human umbilical vein endothelial cells; from Lonza) were starved for 12 h in their own medium at 1% FBS and then seeded in the upper chamber (5×10^3 cells in 200 µl of medium 1% FBS). SMCs and HUVECs were incubated for 2 days or 24 h, respectively, and migrated cells were fixed with 4% paraformaldehyde, stained with 0.25% crystal violet/50% methanol and counted under the microscope. For cell growth assays, RAOSMCs (rat aortic SMCs) and HUVECs were seeded on the upper chambers (5×10^3 cells per transwell) and cultivated with pMØ for 24 h in DMEM-F12 1% FBS or M-199 1% FBS for RAOSMCs and HUVECs, respectively. The cell proliferative ability was then analysed using WST-1 Cell Proliferation Assay (Roche Applied Biosciences) according to the manufacturer's instructions. Alternatively, WT and $Phd2^{+/-}$ pMØ were seeded in the lower chamber of a Transwell and transduced with lentiviral vectors (10^8 TU/ml; Sigma) carrying an shRNA against *Sdf1* (NM_013655.4), *Pdgfb* (NM_011057.3), or a scramble control (purchased from Sigma; TRCN0000178772 for *Sdf1*: 5′-CCGGCTGAAGAACAACAACAGACAA CTCGAGTTGTCTGTTGTTGTTCTTCAGTTTTTTG-3′; TRCN0000042529 for *Pdgfb*: 5′-CCGGGAGTCGAGTTGGAAAGCTCATCTCGAGATGAGCT TTCCAACTCGACTCTTTTTG-3′; SHC002V for the scramble: 5′-CCGGCA ACAAGATGAAGAGCACCAACTCGAGTTGGTGCTCTTCATCTTGTTGTT TTT-3′). Sixty hours after macrophage transduction, SMC migration or growth assays were performed by seeding the SMCs in the upper side of the Transwell as above.

SMC differentiation assay. pMØ were seeded in a 24-well plate with DMEM F-12 5% FBS. Conditioned medium was collected after 2 days and supplemented with 25 mM HEPES. RAOSMCs were seeded in a 24-well plate (80×10^3 cells per well) and incubated for 5 h at 37 °C in a moist atmosphere of 5% CO_2 and 95% air. After 2 h of starvation in DMEM-F12 1% FBS, SMCs were stimulated with conditioned medium from WT and $Phd2^{+/-}$ pMØ. After 24 h, differentiation status of the SMCs was assessed by qPCR.

Macrophage and endothelial cell sorting. For cell sorting of adductor macrophages and endothelial cells, the adductors were dissected, dissociated mechanically, and digested using collagenase I for 45 min at 37 °C. For macrophage sorting, the digested cell suspension was incubated for 15 min with mouse anti-CD16/CD32 mAb (Fc Block, BD-pharmingen) and stained with rat FITC-conjugated anti-F4/80 antibody (Serotec) for 20 min at 4 °C. $CD31^+CD45^-$ endothelial cells were sorted from the digested adductor cell suspension after incubation with rat APC-conjugated anti-CD31 and rat FITC-conjugated anti-CD45 (BD-pharmingen) for 20 min at 4 °C.

BM transplantation and haematological analysis. Balb/c WT and $Phd2^{+/-}$ recipient mice were irradiated with 7.5 Gy. Subsequently, 5×10^6 BM cells from green fluorescent protein$^+$ (GFP^+) WT or GFP^+ $Phd2^{+/-}$ mice were injected intravenously via the tail vein. Femoral artery ligation, treadmill running test and bismuth angiography were performed 5 weeks after BM reconstitution. Red and white blood cell count was determined using a haemocytometer (Cell-Dyn 3700, Abbott) on peripheral blood collected in heparin by retro-orbital bleeding. To assess the effect on arteriogenesis of acute deletion of one *Phd2* allele in macrophages, 5×10^6 BM cells from $Phd2^{Rosa26CreERT;lox/WT}$ mice were transplanted into lethally irradiated WT recipient mice. After 5 weeks, transplanted mice were injected intraperitoneally with tamoxifen (1 mg per mouse; Sigma) or vehicle for 5 days. Femoral artery ligation was performed 10 days after tamoxifen treatment as above.

Statistics. The data were represented as mean ± s.e.m. of the indicated number of measurements. Statistical significance was calculated by two-tailed unpaired *t*-test for two data sets and ANOVA followed by Bonferroni post hoc test for multiple data sets using Prism (GraphPad Inc.), with $P < 0.05$ considered statistically significant.

29. Foo, S. S. *et al.* Ephrin-B2 controls cell motility and adhesion during blood-vessel-wall assembly. *Cell* **124,** 161–173 (2006).
30. Benedito, R. *et al.* The notch ligands Dll4 and Jagged1 have opposing effects on angiogenesis. *Cell* **137,** 1124–1135 (2009).
31. Chen, L. W. *et al.* The two faces of IKK and NF-kappaB inhibition: prevention of systemic inflammation but increased local injury following intestinal ischemia-reperfusion. *Nature Med.* **9,** 575–581 (2003).
32. Lutgens, E. *et al.* Chronic myocardial infarction in the mouse: cardiac structural and functional changes. *Cardiovasc. Res.* **41,** 586–593 (1999).
33. Jordan, B. F., Cron, G. O. & Gallez, B. Rapid monitoring of oxygenation by 19F magnetic resonance imaging: Simultaneous comparison with fluorescence quenching. *Magn. Reson. Med.* **61,** 634–638 (2009).
34. Pfeffer, M. A. *et al.* Myocardial infarct size and ventricular function in rats. *Circ. Res.* **44,** 503–512 (1979).